Journal of Catalysis 234, 2005, 131 - 142

Oxidative dehydrogenation of propane over V/MCM-41 catalysts: Comparison of O_2 and N_2O as oxidants

Evgueni V. Kondratenko*, Maymol Cherian and Manfred Baerns

Institute for Applied Chemistry Berlin-Adlershof

Richard-Willstätter-Str.12, D-12489 Berlin, Germany

Dangsheng Su and Robert Schlögl

Department of Inorganic Chemistry, Fritz-Haber-Institut der Max-Planck-Gesellschaft,

Faradayweg 4-6, 14195 Berlin, Germany

Xiang Wang and Israel E. Wachs

Operando Spectroscopy & Catalysis Laboratory,

Department of Chemical Engineering,

Lehigh University, Bethlehem, PA 18015, USA

* To whom correspondence should be addressed:

Fax: +49 30 63924454. Email: evgenii@aca-berlin.de.

Keywords: Oxidation, dehydrogenation; O_2, N_2O; propane, propene; vanadia, V_2O_5; silica, MCM-41 support.

Abstract

A series of V/MCM-41 catalytic materials was synthesized by impregnation of MCM-41 as well as adding vanadium during the preparation of MCM-41. The nature and distribution of the VO_x species were studied by different spectroscopic techniques (TEM, TPR, *in situ* UV-Vis, and *in situ* Raman). Highly dispersed VO_x species, which can be classified as monomeric and small 2-dimentional VO_x aggregates, are present in materials with a vanadium loading up to 5.3 wt.% V under conditions of the oxidative dehydrogenation of propane (ODP), and are independent of the preparation method. These VO_x species exhibit similar specific catalytic performance in the ODP reaction as a function of vanadium loading or apparent vanadium surface density. Crystalline V_2O_5 nanoparticles, however, are formed for 11.2 wt.% V when the MCM-41 porous structure collapses.

For all V/MCM-41 catalysts used in this study, higher propene selectivity is achieved with N_2O as compared to O_2 at similar degrees of C_3H_8 conversion. The catalytic activity is, however, lower in the presence of N_2O as compared to O_2 because of the weaker oxidizing potential of N_2O relative to O_2 for the re-oxidation of the reduced surface VO_x sites during the ODP reaction. There is no significant difference in propene selectivity between highly dispersed surface VO_x species and crystalline V_2O_5 nanoparticles when N_2O is used as oxidant. In contrast to highly dispersed VO_x on the surface of MCM-41, the crystalline V_2O_5 nanoparticles are not selective for the ODP reaction in the presence of O_2. The positive effect of N_2O is related to the inhibition of direct C_3H_8 oxidation and also the consecutive oxidation of C_3H_6 to CO_x. The inhibition is ascribed to reducing surface density (spatial separation) of active surface lattice oxygen in VO_x species, since N_2O is a weaker oxidant for re-oxidation of reduced VO_x species as compared to O_2. From a stoichiometric point of view of the ODP reaction, selective propene formation is favored over combustion reactions at the lower surface densities.

1 Introduction

Conversion of low alkanes to value-added olefins, the building blocks of the petrochemical industry, by selective oxidative dehydrogenation reactions may become a potential economical route for their production in the coming years if selectivities and yields of olefins are significantly improved. The oxidative dehydrogenation of propane (ODP) to propene has been intensively investigated due to increasing world demand for propene. This reaction is, however, kinetically limited for attaining high propene yields, as the selective reaction product, i.e. propene, is more reactive than propane and is easily combusted in the oxidizing environment [1]. Therefore, designing suitable catalysts and/or a suitable process environment are important challenges in the coming years. Numerous catalytic systems have been evaluated for the ODP reaction and the relevant results have been recently reviewed [2, 3]. Vanadium- and molybdenum-based catalytic materials are claimed to be most active and selective for the ODP reaction with O_2 [4-6]. Supported vanadium oxide catalysts have typically been found to be more selective than the unsupported bulk V_2O_5 material because of the interactions of VO_x species with the oxide support substrates (e.g., Al_2O_3, Nb_2O_5, TiO_2, ZrO_2, SiO_2, etc.) [7-9]. It has been reported that the interaction between the oxide support and the deposited vanadium oxide determines the structure of the resulting surface VO_x species [10]. Dehydrated surface VO_x species have been found to possess VO_4 coordination with one terminal V=O bond, with varying degrees of polymerization on the different supports. At high surface vanadium oxide coverage, crystalline V_2O_5 nanoparticles also exist. The catalytic activity in ODP and the propene selectivity are considered to be a function of these different vanadium oxide species and the specific support used. The factors that govern the catalytic performance of the surface VO_x species, however, are still being debated.

Recent studies on supported vanadium oxide on different mesoporous silicas revealed that such materials are active and selective for the oxidative dehydrogenation of propane and

ethane [11-15]. Mesoporous materials provide high surface areas and, hence, the potential for high dispersion of the catalytic active surface VO_x species. The rate of propene formation appears to vary with the dispersion of these species. Therefore the challenge, , is to achieve maximum dispersion of surface VO_x species. The overall performance of mesoporous supported vanadia catalysts for the ODP reaction is also a function of the chosen reaction conditions. The addition of small amounts of H_2O, CO_2 and N_2O to the ODP reaction feed [16-18] has been found to increase the propene selectivity at the expense of catalytic activity. When CO_2 was employed as the oxidant, the propene selectivity over a gallium oxide catalyst was enhanced [19]. The use of CO_2 as an alternative oxidant, however, is limited due to catalyst coking and byproduct CO formation. Nitrous oxide was also applied as an oxidant for the ODP reaction over supported VO_x/γ-Al_2O_3 [20] resulting in an improved propene selectivity as compared to molecular oxygen. This finding suggests that N_2O may be promising as an oxidant for the ODP reaction.

Based on the above background, the present investigation is focused on understanding the influence of N_2O and O_2 as oxidants on the catalytic performance (activity and selectivity-conversion relationship) of supported V/MCM-41 catalytic materials for the ODP reaction. The effect of preparation methods and vanadium loadings on the distribution of VO_x species on the MCM-41 support among isolated surface VO_4 species, polymeric surface VO_4 species, and crystalline V_2O_5 nanoparticles will be elucidated with the application of different *in situ* spectroscopic methods. This molecular-level information will be used in deriving structure-reactivity-selectivity relationships of V/MCM-41 catalytic materials for the ODP reaction.

2 Experimental

2.1 Catalyst Preparation

Two different preparation methods were chosen for deposition of vanadia on the mesoporous MCM-41 support prepared according to [21]. One type of catalyst was prepared by impregnating MCM-41 with a predetermined amount of vanadium acetyl acetate ($[CH_3COCH=C(O-)CH_3]_2VO$) in toluene. The final mixture was stirred at 300 K for 24 h followed by filtering and washing the impregnated catalyst with toluene to remove weakly bonded VO_x species. The resulting catalyst precursor was subsequently subjected to drying at 400 K for 12 h and calcination at 823 K for 12 h.. The second type of catalyst was prepared using vanadyl sulphate ($VO(SO)_4$) dissolved in water that was mixed with tetraethylorthosilicate (TEOS) and cetyltrimethyl ammonium bromide (CTAB), with the latter being templates used for the preparation of MCM-41 support. The resulting mixture was stirred for 24 h at 300 K and subjected to filtration, drying and calcination procedures as described above. Samples with different amounts of vanadium loadings varying from 0.2 to 11.2 wt. % were synthesized. The catalysts are denoted below by their amount of vanadium loading [e.g. V(2.7)/MCM-41 contains 2.7 wt.% of V in the sample].

2.2 Catalyst Characterization

The surface areas and the final vanadia contents were determined after catalyst calcinations by BET and ICP analysis, respectively. The physical distribution of vanadia over the MCM-41 support was examined with TEM. The molecular distribution among the dehydrated isolated and polymeric surface VO_4 species and crystalline V_2O_5 was studied with *in situ* Raman and *in situ* UV-Vis DRS. Crystalline V_2O_5 nanoparticles greater than 4 nm were subjected to XRD. The reducibility of VO_x species in the supported V/MCM-41 catalysts was investigated

by *in situ* UV-Vis DRS and H_2-TPR. A short description of each of the characterization methods and experimental procedures is given below.

Nitrogen physisorption was employed to obtain specific surface areas in a single point BET analyser (Gemini III 2375, Micromeritics) by using N_2 physisorption at 77 K. The BET values are presented in Table 1. The method of Barret, Joyner and Halenda (BJH) was employed to determine the pore size distribution.

Table 1 Vanadium content, BET surface area and average pore diameter of the synthesized catalysts

Method of catalyst preparation	Vanadium content / wt. %	S_{BET} / m^2/g	Average pore diameter / Å
Addition of vanadium during MCM-41 synthesis	0	1011	25.8
	0.2	1059	25.8
	0.6	892	26.2
	1.2	807	28.1
	2.7	871	27.8
	5.3	790	23.9
Impregnation of MCM-41 with vanadium	3.1	875	28
	4.1	836	27
	11.2	52	380

Inductively coupled plasma (ICP) measurements were used to determine the vanadium concentrations of each catalyst after calcination at 823 K. The final vanadium contents of the different catalysts are presented in Table 1.

Transmission electron microscopy (TEM) investigations of V/MCM-41 catalytic materials were performed for morphology determinations on a Philips CM 200 FEG field emission transmission electron microscope operated at 200 kV in vacuum.

UV Raman spectra were collected using a Jobin Yvon Labram HR (High Resolution) spectrometer system with excitation at 325 nm (0.2 mW) and spectral resolution better than 2 cm^{-1}. The Raman system was equipped with a notch filter to reject the Rayleigh scattering down to ~300 cm^{-1}. The scattered photons were directed and focused onto a single stage monochromator, with 1800 grooves/mm, and a UV sensitive CCD detector maintained at liquid-nitrogen temperature. The *in situ* Raman spectra were taken of the loose samples (10-20 mg) at room temperature after dehydration at 723 K in flowing oxygen (O_2:He=20:80) in an environmental cell (Linkam, model T1600). Visible Raman spectra were collected using a Kaiser Optical Systems RXN spectrometer with excitation at 785 nm.

UV-Vis DRS measurements were performed on a Cary 400 Varian spectrometer equipped with an *in situ* environmental cell (praying mantis, Harrick). The samples were diluted with Al_2O_3 in a 1:10 ratio. The samples for *in situ* measurements were pretreated in an O_2/N_2 (20% O_2) mixture at 773 K for 1 h. After this pretreatment, the *in situ* UV-Vis DRS spectra of the catalytic materials were recorded at 773 K in an atmosphere of either hydrogen (H_2:N_2=10:90) or of propane (C_3H_8:N_2=10:90). The spectra were converted into the Kubelka-Munk function F(R).

X-ray diffraction (XRD) analyses were carried out using a STADIP transmission powder diffractometer (Stoe) with $CuK_{\alpha 1}$ radiation.

H_2-TPR measurements were performed by heating 100 mg of sample with 20 K/min up to 1073 K in a gas mixture of hydrogen (10 vol. % in argon) with a total flow rate of 50 cm^3_{STP} min. Hydrogen consumption was monitored by a thermal conductivity detector (TCD). Water formed or desorbed during TPR measurements was removed by molecular sieve 4Å before the flow entered the TCD. The hydrogen consumption was calibrated by argon pulses continuously introduced into the gas flow during sample heating.

2.3 Catalytic tests

A U-shaped fixed-bed quartz reactor (i.d. 5 mm) was employed for the catalytic tests. The quartz reactor was immersed into a fluidized bed of sand serving as a source of heat. The temperature within the fixed-bed of catalyst particles was measured by an axially movable thermocouple located inside a quartz capillary. Typically, 0.01-0.1 g of catalyst was diluted with similarly-sized quartz particles and charged in the reactor for further temperature control. The oxidative conversion of propane was investigated using a feed of 40 vol.% C_3H_8 and 40 vol.% N_2O in Ne (C_3H_8:N_2O:Ne = 40:40:20) or 40 vol.% C_3H_8 and 20 vol.% O_2 in N_2 (C_3H_8:O_2:N_2 = 40:20:40) at 1 bar. Neon was used to control the formation of N_2 and O_2 in case of N_2O decomposition. The total flow rate and the reaction temperature were varied between 30 - 240 $cm^3_{STP}\cdot min^{-1}$ and 673 - 793 K, respectively. All V/MCM-41 catalysts were slightly deactivating during the first hour of time-on-stream using N_2O as oxidant. Characteristic reaction rates and product selectivities were only determined after reaching pseudo steady state. The feed and products were analysed using an online GC (HP 5800) equipped with Porapak Q and Molecular sieve-5 columns. The contact times were adjusted for achieving propane conversions of less than 4%, which allowed for the determination of the initial propene selectivity and the initial rates of product formation. The rate of propene formation and turn over frequencie (TOF) were calculated according to equations 1 and 2, respectively. The rate unit is $n_{C3H6}\cdot min^{-1}\cdot g^{-1}$, where n_{C3H6} is the number of propene moles, g refers to the catalyst, and TOF is the number of propene molecules formed per V atom and second.

$$r_{C_3H_6} = \frac{F_t}{22400 \cdot m_{cat}} \cdot C(C_3H_6) \quad (1)$$

$$TOF = \frac{r_{C_3H_6}}{n_V} \quad (2)$$

where F_t is the total volumetric flow (ml/s), m_{cat} is the catalyst mass (g), $C(C_3H_6)$ is the propene concentration at the reactor outlet (vol. %), and n_V is the moles of vanadium per gram of catalyst (mol/g).

3 Results

The following three sections describe the results of physical and chemical characterization of the supported V/MCM-41 catalytic materials. The catalytic performance of these materials in the oxidative dehydrogenation of propane in the presence of O_2 and N_2O are subsequently presented.

3.1 Morphology of V/MCM-41 materials as a function of V content and preparation method

The specific surface areas (S_{BET}) of the catalytic materials and the pure MCM-41 support are shown in Table 1. There is only a slight decrease in S_{BET} of the supported V/MCM-41 catalysts for vanadium loadings up to 5.3 wt.%. This is valid for both supported V/MCM-41 and materials prepared by vanadium addition during synthesis of MCM-41. S_{BET} of V(11.2)/MCM-41 is significantly lower than of the other catalytic materials indicating that the microstructure of MCM-41 is influenced by the comparatively high vanadium loading . The average pore size was calculated as ~ 2.7 nm for all the catalytic materials with the exception of V(11.2)/MCM-41. Thus, the mesoporous structure of the support was preserved in most of the synthesized materials. This conclusion is further supported by the results of the morphology as obtained by TEM measurements (Figure 1); the TEM image of the supported V(0.2)/MCM-41 catalyst is shown in Figure 1a where the micrograph is taken with the electron beam parallel to the pores. The TEM image reveals that the highly ordered nanoporous structure of MCM-41 is preserved after loading it with vanadium oxide. Although

X-ray energy dispersive spectroscopy on the TEM reveals the presence of vanadium, the absence of any vanadium oxide contrast in Figure 1a indicates that vanadium oxide must exist in a dimension of less than 1 nm being not detectable in the TEM image. Upon increasing the vanadium loading, no significant changes in the structure of MCM-41 and in the vanadium distribution is observed (Figure 1b). Higher loadings of vanadium cause a dramatic change of the MCM-41 structure as shown for V(11.2)/MCM-41 in Figure 1c: (i) all the nanoporous channels disappear, (ii) the MCM-41 structure undergoes a morphological change by agglomeration to large debris giving the *polymer*-like contrast in Figure 1c, and (iii) V_2O_5 crystals as large as several 10 nm are found in this sample. These morphological changes result in a dramatic drop of S_{BET} from 800-900 (see Table 1) to 52 m^2/g.

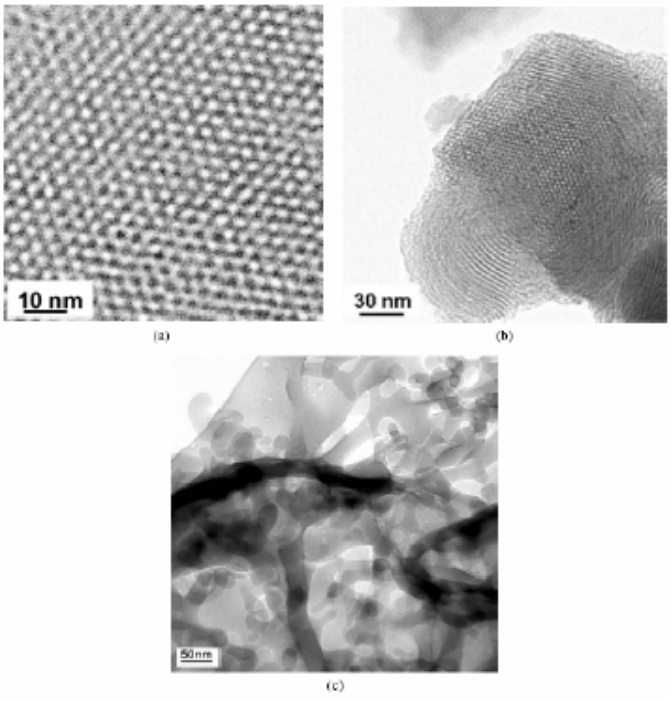

Fig. 1. TEM micrographs of the V/MCM-41 samples taken with the electron beam parallel to the pores: V(0.2)/MCM-41 (a), V(2.5)/MCM41 (b) and V(11.2)/MCM-41 (c)

The effect of vanadium loading on the crystallization of V/MCM-41 materials was also investigated by powder XRD. For samples with vanadium loading up to 5.3 wt.%, no spectral features indicating the presence of crystalline V_2O_5 are present. This may be understood either as the presence of small crystalline nanoparticles (< 4 nm) or as surface VO_x species that cannot be detected by XRD due to the absence of long-range order. Intense reflexes corresponding to crystalline V_2O_5 are, however, visible in the XRD-patterns of V(11.2)/MCM-41 (Figure 2), which is in agreement with the TEM observation shown in Figure 1 c. Raman and UV-Vis spectroscopic characterization studies were also undertaken in order to obtain more definitive information about the possible presence of XRD-amorphous crystalline V_2O_5 nanoparticles and surface VO_x species for samples possessing up to 5.3 wt.% V.

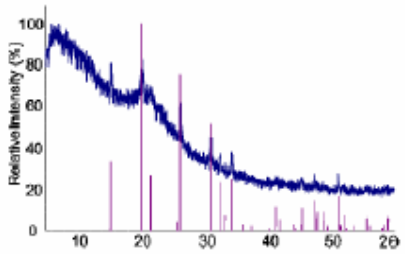

Fig. 2. Powdered X-ray diffraction patterns of V(11.2)/MCM-41.

3.2 *Determination of different VO_x molecular structures and their partitioning in V/MCM-41*

A comparison of the *in situ* UV-Vis spectra of all the V/MCM-41 samples is shown in Figure 3. The spectra were taken at 773 K in a flow of O_2 (O_2:N_2=20:80). Under such conditions water is released from the coordination sphere of V^{5+} leaving behind tetrahedrally coordinated V^{5+}. Thespectra are essentially the same for all dehydrated V/MCM-41 catalysts with the exception of the highly loaded V(11.2)/MCM-41 sample that also contains XRD detectable crystalline V_2O_5 (Section 3.1, Figure 2). The absorption at 295 nm, as well as its correspondingly high band gap energy value (E_g~3.4 eV) is characteristic of isolated

dehydrated surface VO_4 species [22]. In order to derive more precise insights into the structure of VO_x species in low-loaded (≤ 5 wt. %) V/MCM-41 samples, their UV/Vis spectra were compared with those of magnesium vanadates having structures of $Mg_3V_2O_8$ and $Mg_2V_2O_7$, where isolated VO_4 units and VO_x species with V-O-V bonds, respectively, are present. Figure 4 compares these spectra. It is clear that spectra of low-loaded (≤ 5 wt. %) V/MCM-41 samples differ from that of pure $Mg_3V_2O_8$ but they are similar to that of a mixture of $Mg_3V_2O_8$ and $Mg_2V_2O_7$. Taking into account these experimental observations it is concluded that both isolated VO_4 units and small VO_x aggregates having V-O-V bonds are present on the surface of the low-loaded (≤ 5 wt. %) V/MCM-41 samples. Within this manuscript the above VO_x species are called highly dispersed ones. Increasing the vanadium content to 11.2 wt.% gives rise to a new broad UV-Vis band between 400-600 nm, with a corresponding low band gap energy value (E_g~2.9 eV), characteristic of crystalline V_2O_5 [23].

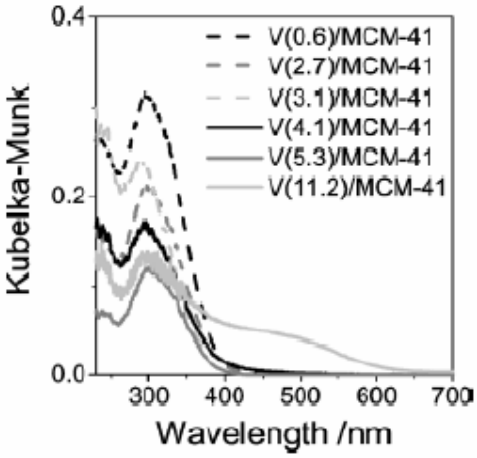

Fig. 3. UV/vis-DRS spectra of different V/MCM-41 materials during pre-treatment in an O_2/N_2=20:80 mixture at 773 K.

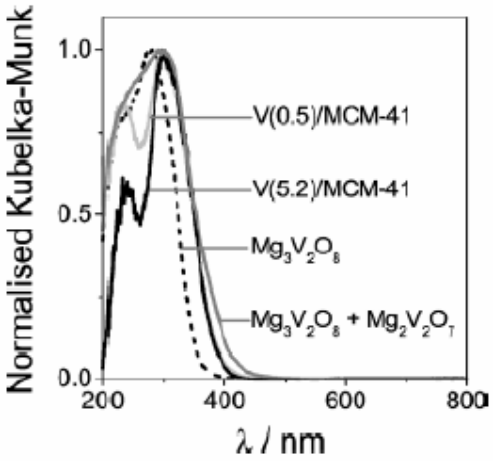

Fig. 4. UV/vis-DRS spectra of V(0.5)/MCM-41 and V(5.3)/MCM-41 materials as well as $Mg_3V_2O_8$ and $Mg_2V_2O_7$.

The *in situ* Raman spectra of the V/MCM-41 catalysts, after dehydration at 723 K, are compared in Figure 5. The spectra in Figure 5 (a) and Figure 5 (b) are taken under 325 nm and 785 nm excitation. The band at ~477 cm^{-1} originates from vibrations of Si-O-Si rings of the MCM-41 support and the band at ~1031 cm^{-1} is associated with dehydrated highly-dispersed surface $O=V(-O-Si)_3$ species [24-26]. However, recent theoretical and experimental studies on Raman spectra of V/SiO_2 provide an indication that the band at ~ 1031 cm^{-1} cannot be assigned to vanadyl species exclusively [27]. It is concluded that the highly dispersed surface VO_x species are in non-framework sites, since no Raman band at ~966 cm^{-1} was identified [28]. The absence of a sharp Raman band at ~994 cm^{-1}, with its multiple associated sharp bands at lower wave numbers, demonstrates that crystalline V_2O_5 nanoparticles are not present in any of the V/MCM-41 samples with vanadium loadings up to 5 wt.%. This band was identified in V(11.2)/MCM-41 only (Figure 5). Since polymeric VO_x-species can be easily detected under visible excitation [28] in contrast to isolated vanadyl species, Raman spectra of V(5.3)/MCM-41 and V(11.2)/MCM-41 samples were collected at 785 nm excitation. The respective spectra are given in Figure 5 (b). This figure shows nicely that

crystalline V_2O_5 nano-particles in the V(11.2)/MCM-41 sample are strongly resonance-enhanced under visible laser excitation. Since no signs of the presence of crystalline V_2O_5 nanoparticles were found in V(5.3)/MCM-41 even under visible laser excitation, it is concluded that V/MCM-41 samples with vanadium loading lower than 5.3 wt.% are free of crystalline V_2O_5 nanoparticles.

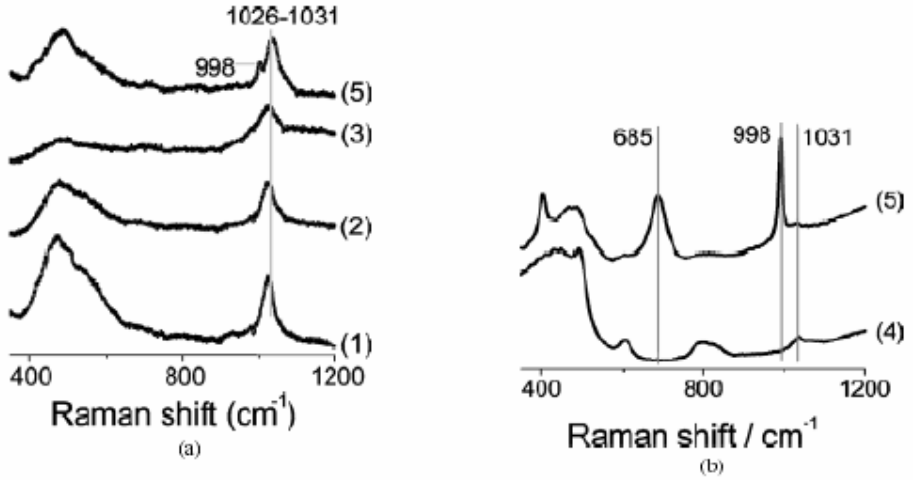

Fig. 5. Raman spectra of different V/MCM-41 materials under dehydrated conditions with 325 (a) and 785 (b) nm excitation wavelengths: (1) V(0.2)/MCM-41, (2) V(2.1)/MCM-41, (3) V(4.1)/MCM-41, (4) V(5.3)/MCM-41, (5) V(11.2)/MCM-41.

3.3 Redox properties

The *in situ* UV-Vis spectra obtained after reduction of fully oxidized V(2.7)/MCM-41 by C_3H_8 or H_2 at 773 K are presented in Figure 6. The intensity of the ligand to metal charge transfer (LMCT) bands in the 200-400 nm region decreases upon exposure to the reducing C_3H_8 as well as H_2 due to reduction of the V^{5+} to V^{4+} or V^{3+}. The UV-Vis bands for surface V^{4+} and/or V^{3+} species arise from d-d transitions and appear as broad and weak features in the 400-700 nm region (note the non-zero value of the absorption for the reduced samples in this region) [22, 29]. The reduced samples were subjected to re-oxidation. The reduced surface VO_x species are easily re-oxidized to the surface V^{5+} species, but the re-oxidation is

incomplete for the chosen experimental conditions (see Figure 6). Similar results are characteristic also for all the V/MCM-41 catalysts.

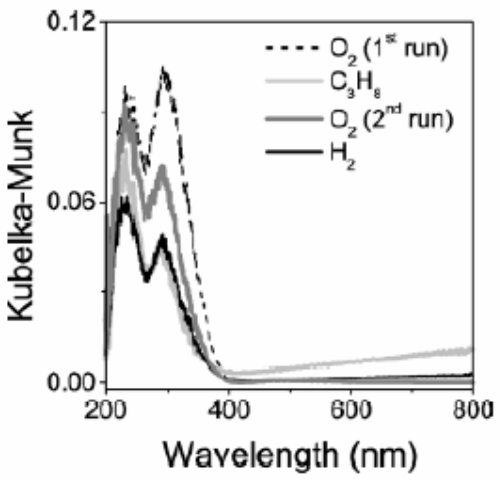

Fig. 6. UV/vis spectra under oxidation and reduction environment at 773 K (O_2/N_2=20:80, C_3H_8/N_2=10:90 and H_2/N_2=10:90).

The H_2-TPR spectra of the V/MCM-41 materials are shown in Figure 7. T_{max} which qualitatively reflects the reducibility of the supported vanadia, increases slightly from 778 to 793 K as the vanadium loading increases from 0.2 to 5.3 wt % for the samples prepared by the addition of vanadium during synthesis of MCM-41. For the impregnated samples, T_{max} is slightly higher and around 808 K. These slight shifts to higher T_{max} are a consequence of the higher H_2O partial pressures formed with higher V loaded samples that retard the reduction process. The single T_{max} obtained for all samples represents a single stage reduction of the surface V^{5+} to surface V^{3+} [29-31]. The H_2-TPR profile for V(11.2)/MCM-41 has an additional shoulder with a maximum shifted to higher temperatures due to the presence of crystalline V_2O_5 nanoparticles in this sample. Higher T_{max} for crystalline V_2O_5 than for the surface VO_x species arises from the more difficult reduction of the internal V^{5+} sites in the V_2O_5 crystalline lattice during H_2-TPR.

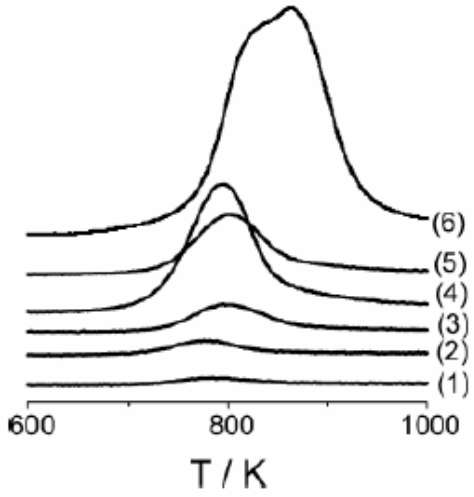

Fig. 7. H_2-TPR spectra for differently prepared V/MCM-41 catalytic materials as a function of V loading: (1) V(0.2)/MCM-41, (2) V(0.6)/ MCM-41, (3) V(1.2)/MCM-41, (4) V(3.1)/MCM-41, (5) V(2.7)/MCM-41, (6) V(11.2)/MCM-41.

3.4 Catalytic performance of V/MCM-41materials with O_2 and N_2O

C_3H_6, CO and CO_2 were the main reaction products using oxygen and nitrous oxide as oxidants in the ODP reaction over the differently loaded and prepared V/MCM-41 catalytic materials. Very small amounts, < 0.01 vol. %, of acetaldehyde and acrolein were also produced as reaction by-products. The effect of V loading, method of catalyst preparation and oxidant was examined for their influence on the rate of propene formation (C_3H_6 moles·min^{-1}·g^{-1}) using oxygen and nitrous oxide as oxidants. The corresponding activity results are plotted in Figure 8 (a) and Figure 8 (b) as a function of the V content and apparent V surface density, respectively. These results reveal that the activity for propene formation is higher with O_2 than with N_2O for all vanadium loadings or surface densities. Independent of the oxidizing agent, the activity increases with increasing vanadium loading up to 5.3 wt.% (ca. 1 V/nm^2). There is no significant difference in the rates of propene formation for samples prepared by different methods. This indicates similarity of VO_x species in differently prepared V/MCM-41 materials. To understand the intrinsic activity of surface VO_x species, the turn over frequency (TOF) was calculated according to equation 2 and is presented in Figure 9.

The nearly constant TOF values for the catalysts with vanadium loadings up to 5.3 wt.% (V surface density is ca.1 V/nm^2) suggest that all the surface VO_x sites are essentially identical. V(11.2)/MCM-41 has the lowest TOF value due to formation of sintered V_2O_5 nanoparticles (dispersion < 100%). The catalytic ODP reaction is sensitive to the specific oxidant and lower TOF values were obtained with N_2O than with O_2. This observation is discussed in detail in section 4.1.

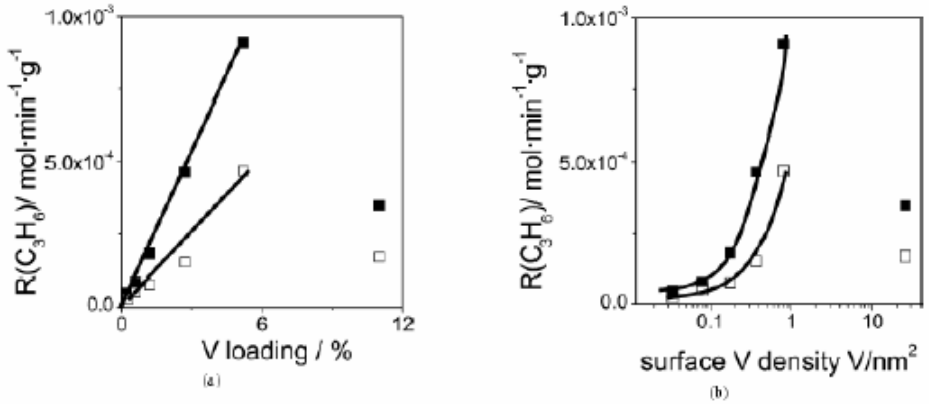

Fig. 8. Rates of propene formation versus vanadium loading (a) and apparent vanadium surface density (b) at 748 K using $C_3H_8/O_2/N_2$=40:20:40 (closed symbols) and $C_3H_8/N_2O/N_2$=40:40:20 (open symbols) mixtures.

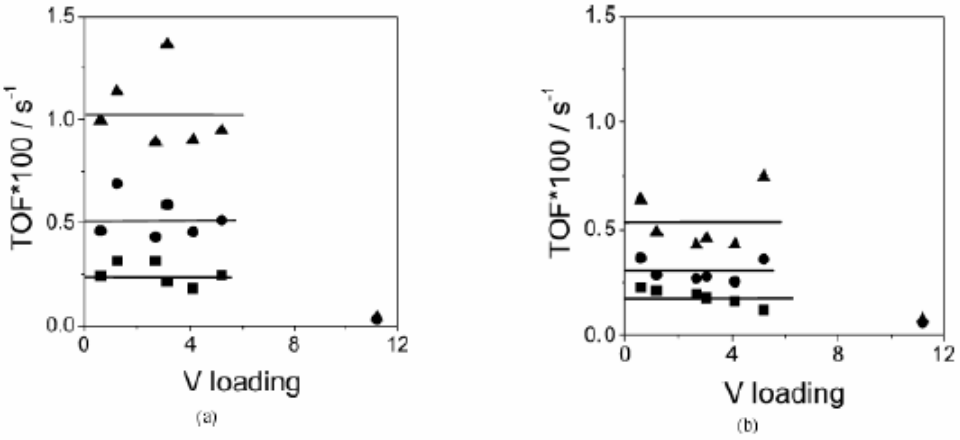

Fig. 9. TOF of propene formation at 698 (●), 723 (■) and 748 (▲) K versus vanadium loading using $C_3H_8/O_2/N_2$=40:20:40 (a) and $C_3H_8/N_2O/N_2$=40:40:20 (b) mixtures.

The effect of vanadium loading and type of oxidant on propene selectivity at a degree of propane conversion of ca. 2% is shown in Figure 10. The selectivity increases slightly with an increase in vanadium loading up to 5.3 wt.% and decreases with further increase in vanadium loading; the selectivity maximum is difficult to define due to lacking experimental data. This is valid for catalytic tests with both N_2O and O_2. However, for an N_2O-containing mixture this decrease is not as clear as that for an O_2-containing reaction feed. It is also to be emphasized that the propene selectivity with N_2O is slightly higher over all the catalysts than that with O_2. Further studies were done to understand the reaction pathways for ODP by conducting the ODP tests with N_2O and O_2 at different contact times, i.e. different degrees of propane conversion. The selectivity-conversion relationships for different catalysts in the presence of O_2 and N_2O are compared in Figure 11. The propene selectivity decreases while CO and CO_2 selectivities increase with increasing propane conversion for both oxidants. The obtained relationship indicates the secondary nature for CO_x formation, i.e. CO and CO_2 are formed via consecutive C_3H_6 oxidation. Taking into account this finding as well as the non-zero CO and CO_2 selectivity at near-to-zero C_3H_8 conversion, it is suggested that both CO_2 and CO can be also primary products of total propane oxidation. However, this reaction pathway plays a significant role at low degrees (< 2%) of propane conversion only. The contribution of the consecutive C_3H_6 oxidation to total CO_x production increases strongly with a progressive increase in C_3H_8 conversion and prevails at high degrees. From a more detailed analysis of the results in Figure 11 it is concluded that CO formation is stronger influenced by the degree of C_3H_8 conversion as compared to CO_2 formation. For an O_2-containing feed, relative changes in CO selectivity over V(2.7)/MCM-41, V(3.1)/MCM-41 and V(11.2)/MCM-41 are 13%, 8% and 15% upon increasing C_3H_8 conversion from 0.8 to 7.6, 1.5 to 7.4 and 2 to 7.5, respectively. Respective changes in CO_2 selectivity are 6%, 5% and 2.7%. By comparing the relative changes in CO and CO_2 selectivities it is obvious that CO selectivity as compared to that of CO_2 is a stronger function of the degree of C_3H_8 conversion. Thus, it is concluded that

propene is largely oxidized to CO as compared to CO_2. The extent of the decrease in propene selectivity, however, is smaller with N_2O than that with O_2. For similar propane conversions, the selectivity towards carbon oxides is ca. 2-3 times higher with O_2 than with N_2O. The above observations suggest a complex reaction scheme of parallel and consecutive steps for the ODP reaction using either O_2 or N_2O; the scheme is presented in Figure 12.

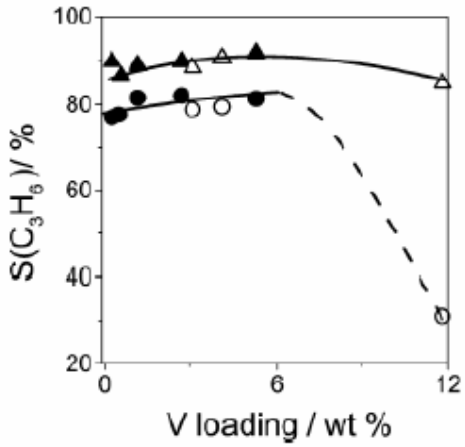

Fig. 10. C_3H_6 selectivity at low degrees of propane conversion (≈2%) at 748 K versus vanadium loading using $C_3H_8/O_2/N_2$=40:20:40 (circles) and $C_3H_8/N_2O/N_2$=40:40:20 (triangles) mixtures. Open symbols are for materials prepared by impregnation, solid symbols are for materials prepared with vanadium addition during MCM-41 synthesis.

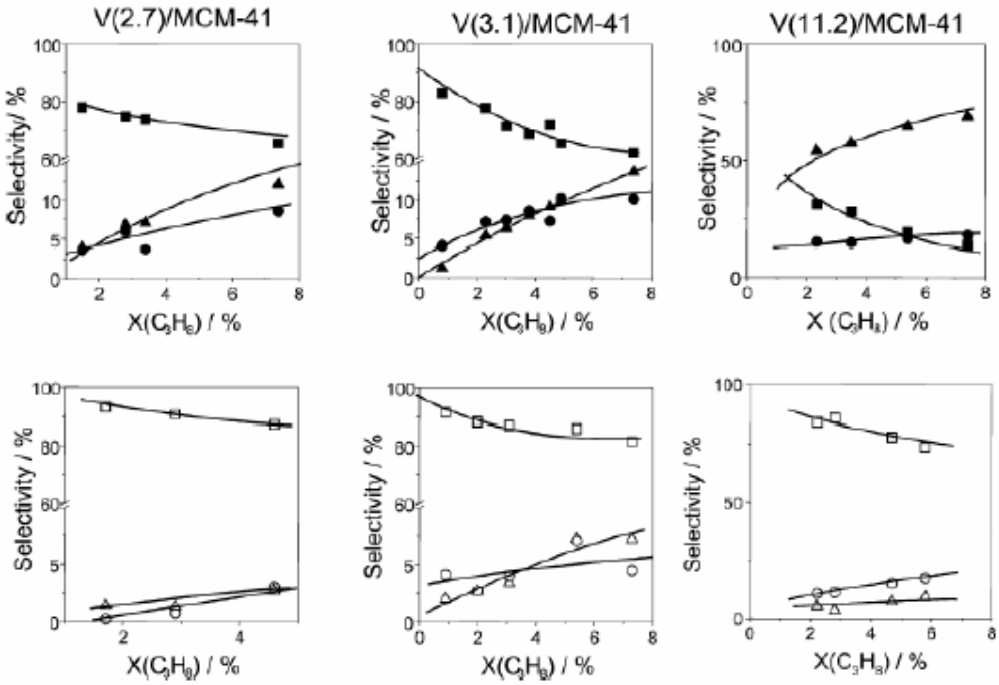

Fig. 11. C_3H_6 (■,□), CO (▲,△) and CO_2 (●,○) selectivities versus propane conversion at 773 using $C_3H_8/O_2/N_2$=40:20:40 (solid symbols) and $C_3H_8/N_2O/N_2$=40:40:20 (open symbols) mixtures.

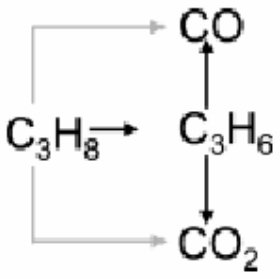

Fig. 12. Suggested reaction scheme of propane oxidation. Solid black arrows represent main reactions, while the grey arrows represent minor reaction pathway.

4 Discussion

4.1 Nature of surface VO_x species and their relationship to the activity and selectivity in the ODP reaction

The results of materials characterization revealed that highly dispersed surface VO_x species are present in the supported V/MCM-41 catalysts up to 5 wt.% V. These species reside in extra-framework positions since the characteristic 960 cm^{-1} band typical for framework cations in siliceous molecular sieves [28] is not observed for the supportedV/MCM-41 catalysts. The molecular structure of the surface VO_x species on MCM-41 is independent of the synthesis method since the same structure results from either incorporation during the MCM-41 synthesis process or by post-impregnation of the formed MCM-41 support (Section 3.2). This agrees well with previously reported results on characterization of V/MCM-41 [13, 32], V/MCM-48 [22] and V/HSM silica [33]. The Raman spectra suggest that all the vanadia species are located in accessible surface sites since these dehydrated sites readily become hydrated upon exposure to ambient air [29]. The V(11.2)/MCM-41 sample, however, consists of a collapsed MCM-41 structure and crystalline V_2O_5 nanoparticles.

The experimental data showed that the catalytic performance (i.e., activity and the relationship between propene selectivity and propane conversion) of V/MCM-41 catalysts in the oxidative dehydrogenation of propane depends on the distribution of VO_x species on the catalyst surface and the nature of the oxidant. From Figure 10 it can be seen that the propene selectivity at propane conversion of ca 2 % increases slightly with vanadium loadings up to 5.3 wt. % for both oxidants. The weak differences in C_3H_6 selectivity of catalysts with low vanadium loadings (up to 5.3 wt%) is a strong indication on the participation of surface VO_x species of the same nature in C_3H_8 activation yielding C_3H_6. This is supported by the results from characterization techniques, such as, UV-Vis and Raman spectroscopy (Section 3.2), which demonstrate the presence of highly dispersed surface VO_x in these samples. For

V(11.2)/MCM-41, which possesses crystalline V_2O_5 nanoparticles (section 3.2), there is only a slight decrease in propene selectivity from ca. 90 % to 85 % when N_2O is used while for O_2 there is a marked decrease from ca. 80 % to 30 % at comparable degrees of propane conversion. A possible reason for these phenomena is presented and discussed in section 4.2.

As shown in Figure 8, the rate of C_3H_6 formation and the TOF values are lower with N_2O than with O_2 as oxidant. This can be explained in the following way. It is commonly accepted that the ODP reaction over vanadia-based catalysts proceeds via a Mars-van Krevelen mechanism. This mechanism suggests that C_3H_8 removes lattice oxygen from VO_x species yielding C_3H_6, H_2O and a reduced VO_x center (equation 3). Subsequently, the lattice oxygen is replenished by gas-phase oxygen in a re-oxidation step (equation 4). In the case of N_2O, the catalyst re-oxidation proceeds according to equation 5. The reactions steps involved are assumed to be irreversible. In our previous work on the ODP reaction over VO_x/γ-Al_2O_3, it was shown, that the same oxygen species, i.e. lattice oxygen of vanadia, is formed from O_2 and N_2O [20].

$$C_3H_8 + [O] \xrightarrow{k_{C_3H_8}} C_3H_6 + H_2O + [\ ] \qquad (3)$$

$$O_2 + 2\ [\ ] \xrightarrow{k_{O_2}} 2\ [O] \qquad (4)$$

$$N_2O + [\ ] \xrightarrow{k_{N_2O}} [O] + N_2 \qquad (5)$$

where [O] stands for lattice oxygen of vanadia and [ ] corresponds to an anion vacancy after removing of lattice oxygen from VO_x species. Under steady-state conditions and in the presence of O_2 and N_2O, the rate of C_3H_6 formation can be described by equations 6 and 7, respectively.

$$r_{C_3H_6}^{O_2} = k_{C_3H_8} \cdot p(C_3H_8) \cdot \left[\frac{1}{1 + \frac{k_{C_3H_8} \cdot p(C_3H_8)}{k_{O_2} \cdot p(O_2)}} \right] \quad (6)$$

$$r_{C_3H_6}^{N_2O} = k_{C_3H_8} \cdot p(C_3H_8) \cdot \left[\frac{1}{1 + \frac{k_{C_3H_8} \cdot p(C_3H_8)}{k_{N_2O} \cdot p(N_2O)}} \right] \quad (7)$$

Besides the product of the C_3H_8 partial pressure and the reaction constant of propane activation equations 6 and 7 include a complex expression (squared brackets). Since the product of the C_3H_8 partial pressure and the reaction constant of propane activation is the same in equations 6 and 7, it cannot be responsible for differences in the rates of C_3H_6 formation with O_2 and N_2O (Figure 8). Therefore, the expression in squared brackets contains information on factors influencing the catalytic activity with both O_2 and N_2O. The lower the denominator in this expression the higher is the rate of propene formation. Two experimental facts should be taken into account: i) k_{C3H8} is the same for O_2 and N_2O containing mixtures; and ii) the ratios of $p(C_3H_8)/p(O_2)$ and $p(C_3H_8)/p(N_2O)$ are 2 and 1, respectively. From equations 6 and 7 as well as the two above facts, a lower reaction rate with O_2 as compared to N_2O would be expected if k_{N2O} and k_{O2} would be the same or k_{N2O} is greater than k_{O2}. However, it would contradict the experimental observations in Figure 8 and Figure 9. Therefore, the lower rate of C_3H_6 formation in the presence of N_2O as compared to that in the presence of O_2 is related to the lower ability of N_2O to re-oxidize the reduced surface VO_x sites. Previously, this low activity of N_2O was experimentally proven for differently loaded catalytic materials of the type VO_x/γ-Al_2O_3 [20]. Taking this into account, the lower intrinsic activity (TOF) of VO_x species for C_3H_8 activation with N_2O than with O_2 (see Figure 9), can be explained as follows. For the calculation of TOF values, the total number of vanadium

atoms (including those in the bulk) was used without considering the fact that not vanadium atoms, but the lattice oxygen of VO_x species participate in C_3H_8 activation. According to equations 3-7, the steady-state concentration of lattice oxygen is a function of the rates of catalyst reduction and re-oxidation. Since the rate of catalyst re-oxidation by N_2O is slower than that by O_2, a lower steady-state concentration of lattice oxygen being responsible for C_3H_8 activation is expected in the presence of N_2O. Therefore, the TOF values presented in Figure 9 do not reflect the discrepancy in the intrinsic activity of VO_x species for the ODP reaction with O_2 and N_2O, but the difference in the ability of the catalyst for its re-oxidation by different oxidants, i.e. differences in steady-state concentrations of lattice oxygen in the presence of two different oxidants. Thus, it is concluded, that the intrinsic activity of VO_x species does not depend on the oxidant used and the rate of re-oxidation by the oxidants is responsible for the different ODP reactivities with O_2 and N_2O.

4.2 Role of oxidant in selective and non-selective routes of ODP

As shown in section 3.4, the selectivity (distribution of products) of the ODP reaction strongly depends on the nature of the oxidant applied (Figure 10 and 11). Although propene is the main olefin with both N_2O and O_2, the propene selectivity achieved is lower when O_2 is used as the oxidant as compared to N_2O. Similar results were previously reported in [20] for the oxidative dehydrogenation of propane over differently loaded VO_x/γ-Al_2O_3 catalytic materials. Two important improving effects of N_2O on the ODP reaction should be especially emphasized: i) a higher primary C_3H_6 selectivity is achieved and ii) the decrease in C_3H_6 selectivity with increasing degree of propane conversion is less marked.

This effect of the oxidant on the catalytic performance can be associated with the activation of the oxidant. As discussed in section 4.1, N_2O re-oxidizes reduced VO_x sites slower as compared to O_2, yielding lower concentration of active lattice oxygen and therefore, its lower density. From the stoichiometric requirements of the ODP reaction it is postulated, that one

selective catalyst site should contain one to two active lattice-oxygen anions to obtain the desired propene. Active sites having more than two active lattice oxygen anions would favor the formation of waste products, i.e. CO and CO_2, by consecutive total oxidation steps . Since, several oxygen species are needed for CO_x formation in contrast to C_3H_6 formation, the latter reaction pathway prevails at low densities/concentration of active oxygen species. This is schematically illustrated in Figure 13. According to this figure CO_x formation is favored at high densities of active lattice oxygen in VO_x surface species. Such a situation occurs, when the rate of catalyst re-oxidation (equations 4 and 5) if faster than that of reduction (equations 3). As discussed in section 4.1, N_2O re-oxidizes reduced VO_x sites slower as compared to O_2, yielding lower concentration of active lattice oxygen, i.e., its surface density is lower. This is particularly valid for V(11.2)/MCM-41, since it has the highest surface density of lattice oxygen in the presence of O_2 and respectively the lowest propene selectivity. The influence of the surface density of active lattice oxygen in VO_x species on propene selectivity is clearly visible for this catalyst as compared to other materials (Figure 10, Figure 11). Thus, spatial separation of active lattice oxygen anions from each other on the catalyst surface favors propene formation and simultaneously minimizes its further oxidation to CO_x. Such a hypothesis of active site isolation in selective oxidation of hydrocarbons was first formulated and published by Callahan and Grasselli [34]. However, in the present discussion, it cannot be excluded that besides lattice oxygen, adsorbed oxygen species also participate in the oxidation of surface intermediates to CO_x as recently shown for a complex mixed-oxide catalyst [35]. In this case, active sites containing one to two lattice oxygen anions may become active for CO_x formation, if additional-adsorbed oxygen species are formed in the vicinity of these selective active sites. A detailed understanding of the role of adsorbed oxygen species is still needed and is presently worked on.

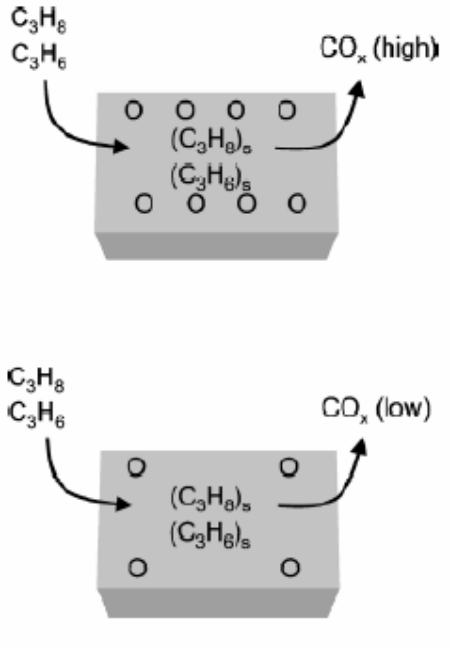

Fig. 13. Schematic presentation of the role of lattice oxygen isolation in CO_x formation.

5 Summary and Conclusions

The findings from the present investigation are summarized :

1. Combination of the characterization results obtained from different techniques (TEM, TPR, in-situ UV/Vis DRS and Raman spectroscopy) for vanadia supported on high-surface-area mesoporous MCM-41 reveals that the nature and distribution of VO_x species does not depend on vanadium loading up to at least 5.3 wt.%. In these samples the VO_x surface species are highly dispersed as monomeric and small surface VO_x clusters under conditions of the oxidative dehydrogenation of propane (ODP). Crystalline V_2O_5 nanoparticles are formed on V/MCM-41 with 11.2 wt.% vanadium when the mesoporous structure collapses.
2. Irrespective of vanadium loading (up to 5.3 wt %), the highly dispersed surface VO_x species show similar intrinsic catalytic activity. However, the measured activity of these species is lower when using N_2O as oxidant in comparison to O_2. The difference is due to the lower ability of N_2O to re-oxidize reduced VO_x species than re-oxidation by O_2.

3. In contrast to highly dispersed surface VO_x species, the crystalline V_2O_5 nanoparticles are not selective when O_2 is used as oxidant. However, in the presence of N_2O, there is no strong difference in propene selectivity.
4. For all the V/MCM-41 materials, the usage of N_2O instead of O_2 favours selective propane oxidation to propene over total combustion of propane or propene. The improving effect of N_2O is related to site isolation of the active surface lattice oxygen species; hereby the direct deep propane and consecutive propene oxidation to CO_x is inhibited.
5. For catalyst design it appears important to ascertain a high dispersion of the reducible metal oxides (MeO_x) on an inert support. These metal oxides should be easily reduced by hydrocarbon than re-oxidised by oxidant. This will spatially isolate active lattice oxygen species in MeO_x aggregates favouring selective oxidation over combustion reaction. With respect to process design it is well known that N_2O is also a suitable oxidant for selective benzene oxidation to phenol. Whether such a process operation can be also applied to selective alkane oxidation remains to be seen. Besides activity and selectivity improvements need to be achieved, availability of N_2O in sufficient quantities has to be ascertained and finally process economics have to be studied.

Acknowledgement The authors from the German institutions gratefully acknowledge financial support by Deutsche Forschungsgemeinschaft (DFG) through the Competence Network "Transition Metal-Oxides Aggregates" (Sfb-546). The work at Lehigh University was supported by the Department of Energy-Basic Energy Sciences (grant DEFG02-93ER14350). The authors from ACA acknowledge Angelika Brückner's help in discussions and for providing Raman spectra obtained under visible excitation.

6 References

[1] H.H. Kung, Adv. Catal. 40 (1994) 1.

[2] O.V. Buyevskaya, M. Baerns, Catalysis 16 (2002) 155.

[3] M. Baerns, G. Grubert, E.V. Kondratenko, D. Linke, U. Rodemerk , Oil Gas-Eur. Mag. 1 (2003) 36.

[4] R.B. Watson, U.S. Ozkan, J. Catal. 191 (1999) 12.

[5] Y. Liu, G. Zhou, M. Xian, Y. Bi, K. Zhen, React. Kinet. Catal. Lett. 73 (2001) 199.

[6] C. Pak, A.T. Bell, T.D. Tilley, J. Catal. 206 (2002) 49.

[7] X. Gao, Q. Xin, X. Guo, Appl. Catal. A 114 (1994) 197.

[8] T.C. Watling, G. Deo, K. Seshan, I.E. Wachs, J.A. Lercher, Catal. Today 28 (1996) 139.

[9] T. Blasco, A. Galli, J.M. López-Nieto, F. Trifiro, J. Catal. 169 (1997) 203.

[10] A. Khodakov, B. Olthof, A.T. Bell, E. Iglesia, J. Catal. 181 (1999) 205.

[11] J.M. López-Nieto, Topics in Catalysis 15 (2001) 189.

[12] O.V. Buyevskaya, A. Brückner, E.V. Kondratenko, D. Wolf, M. Baerns, Catal. Today 67 (2001) 369.

[13] B. Solsona, T. Blasco, J.M. López-Nieto, M.L. Pena, F. Rey, A. Vidal-Moya, J. Catal. 203 (2001) 443.

[14] Y. Wang, Q. Zhang, Y. Ohishi, T. Shishido, K. Takehira, Catal. Lett. 72 (2001) 215.

[15] Q. Zhang, Y. Wang, Y. Ohishi, T. Shishido, K. Takehira, J. Catal. 202 (2001) 308.

[16] W. Schuster, J.P.M. Niederer, W.F. Hoelderich, Appl. Catal. A 209 (2001) 131.

[17] S. Ge, C. Liu, S. Zhang, Z. Li, Chem. Eng. J. 94 (2003) 121.

[18] F. Dury, M.A. Centeno, E.M. Gaigneaux, P. Ruiz, Catal. Today 81 (2003) 95.

[19] P. Michorczyk, J. Ogonowski, Appl. Catal. A 251 (2003) 425.

[20] E.V. Kondratenko, M. Baerns, Appl. Catal. A 222 (2001) 133.

[21] G. Grubert, J. Rathousky, G. Schulz-Ekloff, M. Wark, A. Zukal, Micropor. Mesopor. Mat. 22 (1998) 225.

[22] M. Baltes, K. Cassiers, P. Van Der Voort, B.M. Weckhuysen, R.A. Schoonheydt , E.F. Vansant , J. Catal. 197 (2001) 160.

[23] X. Gao, I.E. Wachs, J. Phy.Chem. B 104 (2000) 1261.

[24] I.E. Wachs, Catal. Today 27 (1996) 437.

[25] I.E. Wachs, J.-M. Jehng, G. Deo, B.M. Weckhuysen, V.V. Guliants, J.B. Benziger, S. Sundaresan, J. Catal. 170 (1997) 75.

[26] I.E. Wachs, in *Catalysis*, J.J. Spivey, Editor. 1997, The Royal Society of Chemistry: Cambridge. p. 37.

[27] N. Magg, B. Immaraporn, J.B. Giorgi, T. Schroeder, M. Bäumer, J. Döbler, Z. Wu, E. Kondratenko, M. Cherian, M. Baerns, P.C. Stair, J. Sauer, H.-J. Freund, J. Catal. 226 (2004) 88.

[28] C.-B. Wang, G. Deo, I.E. Wachs, J. Catal. 178 (1998) 640.

[29] X. Gao, S.R. Bare, B.M. Weckhuysen, I.E. Wachs, Journal of Physical Chemistry B 102 (1998) 10842.

[30] M.M. Koranne, J.G. Goodwin, G. Marcelin, J. Catal. 148 (1994) 369.

[31] F. Arena, N. Giordano, A. Parmaliana, J. Catal. 167 (1997) 66.

[32] H. Berndt, A. Martin, A. Brückner, E. Schreier, D. Müller, H. Kosslick, G.H. Wolf, B. Lücke, J. Catal. 191 (2002) 384.

[33] R. Zhou, Y. Cao, S. Yan, J. Deng, Y. Liao, B. Hong, Catal. Lett. 75 (2001) 107.

[34] J.L. Callaham, R.L. Grasselli, AIChE J. 9 (1963) 755.

[35] E.V. Kondratenko, M. Cherian, M. Baerns, Catal. Today 99 (2005) 59.